

HIGH TEMPERATURE MICROSTRUCTURAL STABILITY OF A MA/ODS FERRITIC ALLOY

M.K. Miller, D.T. Hoelzer, S.S. Babu, E.A. Kenik, and K. F. Russell

Metals and Ceramics Division,
Oak Ridge National Laboratory, Oak Ridge, TN 37831-6136, USA

Abstract

Mechanical alloying of fine pre-alloyed (Fe-12.3 wt% Cr-3% W-0.39% Ti) metal and yttria powders has been shown to produce oxide dispersion-strengthened ferritic alloys with dramatically improved high temperature mechanical properties. Atom probe tomography has revealed that the improved high temperature mechanical properties are correlated with the presence of ultra-stable 4-nm-diameter Ti-, Y- and O-enriched particles. These ultra-fine particles were stable during long-term creep experiments for times in excess of 14,000 h at 800 °C and also during annealing at temperatures of up to 1300 °C. The Y and O levels in the ferrite matrix were significantly higher than the equilibrium levels. These results may be related to the O-Ti, O-W, O-Y and O-Cr solute atom interactions influencing solute diffusion.

Introduction

Ferritic alloys generally do not exhibit good mechanical properties at elevated temperatures. Therefore, ferritic alloys are limited to relatively low-temperature applications. The mechanical properties of ferritic alloys are limited by the rapid decrease of the yield strength at temperatures above ~550°C. The decrease in yield strength is in part associated with recovery of the dislocation substructure produced by prior deformation or phase transformation. This temperature limitation may be extended in some advanced martensitic/ferritic steels by alloying additions that provide a combination of solid solution and carbide precipitation strengthening. Recently, mechanical-alloying (MA) of fine pre-alloyed ferritic metal and Y₂O₃ powders has also been shown to produce oxide dispersion-strengthened (ODS) ferritic alloys with dramatically improved high temperature mechanical properties [1-6]. In addition to permitting alloys to be fabricated from immiscible or low solubility phases, mechanical alloying produces a large amount of deformation and a high dislocation density. Therefore, these alloys are far from thermodynamic equilibrium. Since the powders used in the preparation of the alloy have a relatively large surface-to-volume ratio, a significant amount of surface oxide may be introduced into the alloy, thereby increasing the oxygen level. Therefore, the oxygen level in these mechanically alloyed materials is significantly higher than in alloys produced by conventional casting methods since the majority of the reactive oxygen is not removed as oxides in the liquid state.

In this study, the microstructure of these MA/ODS alloys has been characterized with atom probe tomography in order to understand the origins of the improved mechanical properties. Some previous atom probe tomography characterization of these MA/ODS materials have revealed the presence of ultra-fine Ti-, Y- and O-enriched particles and solute segregation of Cr, W, Ti, Y, O, C and B to dislocations [7-10].

Experimental

Two MA/ODS alloys of nominal compositions Fe-12.3 wt % Cr-3% W-0.24% Y₂O₃ {Fe-13.4 at. % Cr, 0.92% W, 0.12% Y and 0.18% O} (12YW) and Fe-12.3 wt% Cr-3% W-0.39% Ti-0.25% Y₂O₃ {Fe-13.3 at. % Cr, 0.92% W, 0.46% Ti, 0.13% Y and 0.19% O} (12YWT) were examined in this study. These alloys were prepared by milling 70- μ m-diameter pre-alloyed metal and 20-nm-diameter Y₂O₃ powders in a high-energy attritor mill for 48 h under an argon atmosphere [2-5,8]. The mechanically alloyed flakes were then degassed for 2 h at 400 °C in vacuum at a pressure of $< 2 \times 10^{-2}$ Pa, canned in mild steel and then consolidated into bar by hot extrusion at 1150 °C. The alloys were hot rolled at 1150 °C into 7-mm sheet, warm rolled at 600 °C to 2.7 mm sheet and then annealed for 1 h at 1050 °C in vacuum. These alloys were examined in the as-processed condition, after thermal ageing and after creep tests at several elevated temperatures, as summarized in Table 1.

Table 1. Heat treatments and creep results of the 12YW and 12YWT steels.

Alloy	Condition	Temperature, °C	Stress, MPa	strain, %	Time, h
12YW	As processed Heat treated	1300			10
12YWT	As processed Crept Crept Crept Crept Heat treated	650 800 850 850 1300	276 138 173 35+69+104	<2.5 2.2 ~1.3 4.6	13,000 14,235 118 1500+1500+500 10

Atom probe tomography characterizations were performed with the Oak Ridge National Laboratory's energy-compensated optical position-sensitive atom probe [11]. The experimental conditions used for the analyses were a specimen temperature of 50-60K, a pulse repetition rate of 1.5 kHz, and a pulse fraction of 20% of the standing voltage. All compositions are given in atomic percent.

The atoms that were associated with each particle were determined with the maximum separation method [11, 12]. This method is based on the principle that the solute atoms in a solute-enriched particle are closer together than the solute atoms in the solute-depleted matrix [12]. Therefore, a critical distance between solute atoms can be used to apportion the atoms between the particles and the matrix. The composition of each particle was estimated with the envelope method [11]. The Guinier radius of each particle was estimated from the positions of the atoms in the particle, as defined by the maximum separation method [11].

Results and Discussion

The results of the creep tests on the 12YWT alloy are included in Table 1. These results indicate a dramatic improvement in the high temperature creep over other ferritic alloys. The 0.2% yield stress and total elongation from room temperature to 900°C are shown in Table 2 for the as-processed 12YW and 12YWT ODS steels [13]. The strength of the 12YWT steel is

considerably higher than that of the 12YW steel over the entire temperature range from room temperature to 900°C. The high strength of the 12YWT alloy also results in generally lower total elongations compared to the 12YW steel over the temperature range. However, the 12YWT steel shows good ductility despite the higher strength. The different tensile property behavior between 12YWT and 12YW steels will later be attributed to differences in particle dispersions in the microstructures.

Table 2. The 0.2% yield stress and total elongation of the 12YW and 12YWT ODS steels at different test temperatures [13].

Test Temperature °C	Yield Stress, MPa		Elongation, %	
	12YW	12YWT	12YW	12YWT
25	926	1186	12.7	5.1
550	615	865	7.8	8.7
600	513	734	15.8	9.8
650	407	440	18.2	12.3
700	259	405	20.0	20.0
750	218	326	26.0	17.5
800	172	285	24.5	10.9
900	116	178	22.5	10.0

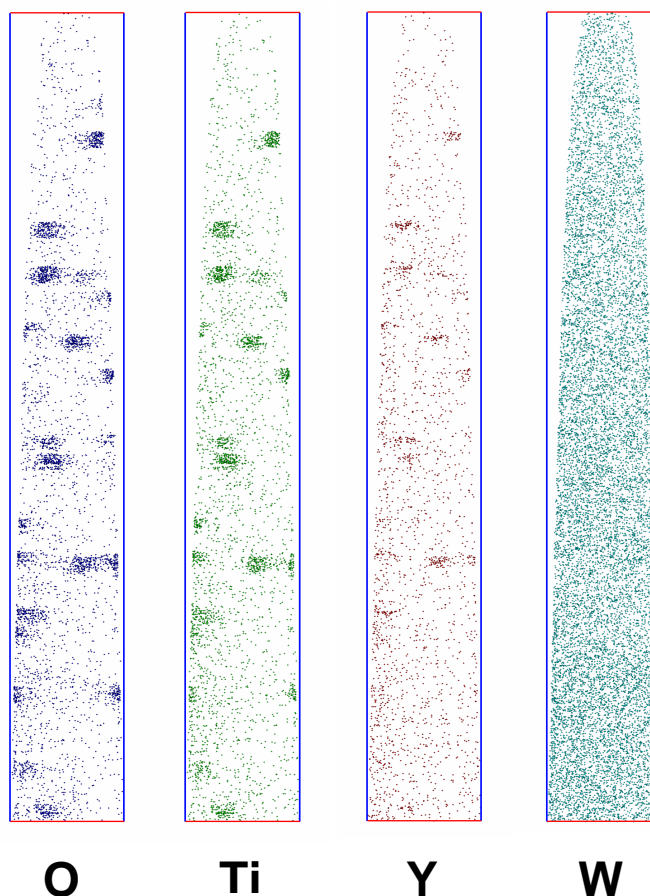


Fig. 1. Atom maps of the solute distribution in 12YWT after 10 h at 1300 °C. A high number density of Ti-, Y- and O-enriched particles is evident.

A representative set of atom maps of the solute distribution for the 12 YWT material heat treated for 10 h at 1300 °C is shown in Fig. 1. A high number density of ultra-fine titanium-, yttrium- and oxygen-enriched particles is evident in all conditions tested except for the 12YW material heat treated for 10 h at 1300 °C. Further characterization of this 12YW material is required to determine if the particles have coarsened significantly at this elevated temperature and the particle number density is too low to be detected with atom probe tomography. It remains unresolved whether the particles have dissolved into the matrix, or whether the solute in the particles has been consumed by some other microstructural feature such as coarse oxides, dislocations or grain boundaries.

The Guinier radius and number density of these ultra-fine particles were determined from the atom probe tomography data. The results are summarized in Table 3. The radius of the particles of approximately 2 nm was found not to change during any of the creep test or during isothermal ageing for 10 h at 1300 °C, indicating the extreme stability these particles. A radial concentration profile from the center of mass of a particle into the matrix is shown in Fig. 2. The concentration profile shows that yttrium is depleted in the center of the particle and enriched at the interface.

Table 3. The average Guinier radii, r_G , and number densities of the particles for each condition, as estimated by the maximum separation method.

Alloy	Condition	r_G , nm	Number Density, m^{-3}
12YW	as processed	2.4 ± 0.9	3.9×10^{23}
	10 h at 1300 °C	-	Not observed
12YWT	as-processed	2.0 ± 0.8	1.4×10^{24}
	Crept 650 °C	2.0 ± 0.8	1.3×10^{24}
	Crept 800 °C	2.0 ± 0.8	9.9×10^{23}
	Crept 850°C (multi-step)	2.0 ± 0.7	9.8×10^{23}
	Crept 850 °C	1.9 ± 0.4	8.3×10^{23}
	10 h at 1300 °C	2.0 ± 0.6	3.8×10^{23}

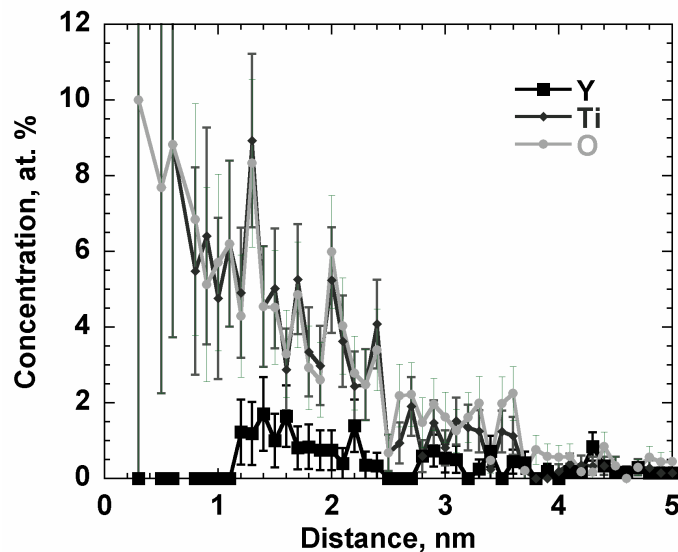


Fig. 2. Radial concentration profiles from the center of mass of a particle into the matrix for the 12YWT alloy heat treated for 10 h at 1300 °C.

Table 4. The average composition of the particles, as determined by the envelope method. The balance of these analyses was iron.

Particles (average of individual compositions)		Cr	W	Y	Ti	O
12YW	As-processed	14.5 ± 5.5	0.19 ± 0.19	21.2 ± 9.4	1.41 ± 1.5	11.4 ± 10.7
12YWT	As-processed	7.0 ± 4.3	0.21 ± 0.21	9.22 ± 7.8	19.9 ± 8.7	23.6 ± 10.6
	Crept 650°C	7.8 ± 4.5	0.12 ± 0.12	7.60 ± 7.3	21.4 ± 8.9	23.8 ± 8.1
	Crept 800°C	5.6 ± 3.9	0.33 ± 0.33	7.89 ± 4.9	24.6 ± 8.5	28.1 ± 9.8
	Crept 850°C -MS	7.2 ± 4.7	0.45 ± 0.98	10.9 ± 9.4	17.2 ± 8.2	21.7 ± 10.8
	Crept 850°C	7.8 ± 4.1	0.33 ± 0.29	5.68 ± 3.0	23.6 ± 7.5	24.6 ± 8.1
	10 h 1300°C	6.5 ± 4.5	0.73 ± 0.73	9.75 ± 9.1	13.5 ± 7.1	21.2 ± 10.5

The average composition of the particles as estimated by the envelope method is summarized in Table 4 for all the conditions examined. As indicated in the atom maps, these particles are enriched in titanium, oxygen and yttrium. The particles also exhibited high iron content. The average titanium + yttrium to oxygen ratio (M:O) was ~1 for all the 12YWT materials but ~3 in the 12YW material. The significant difference between these ratios and that (0.66) of the original Y_2O_3 powder indicate that these particles are not remnant of the 20 nm powder. The variation in the composition of the particles is illustrated in the results from the 12YWT material heat treated for 10 h at 1300 °C in Fig. 3. Similar variations were observed for the other conditions. The smaller particles were found to be richer in oxygen than the larger ones.

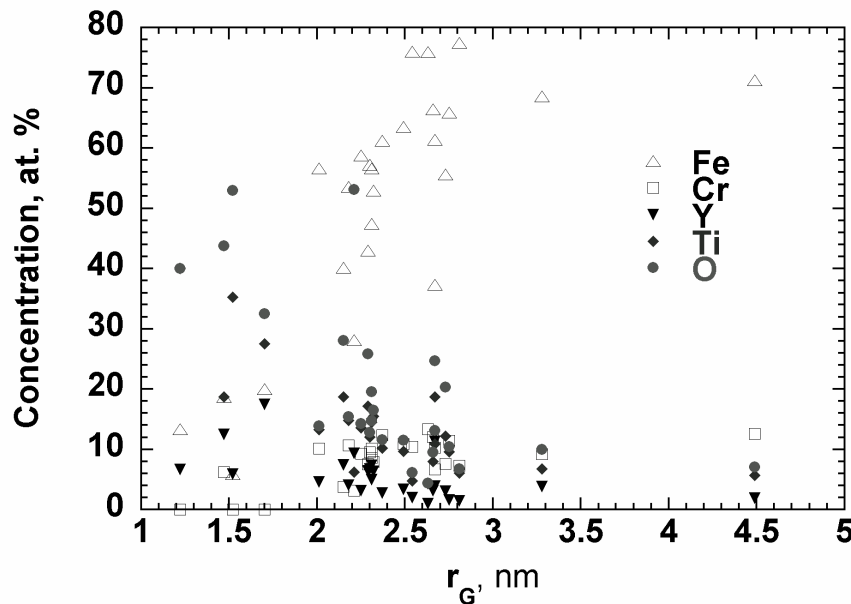


Fig. 3. The variation in the composition of the Ti-, Y-, and O-enriched particles as a function of particle size for the 12YWT material thermally aged for 10 h at 1300 °C.

The matrix composition for all conditions examined is summarized in Table 5. Significant amounts of the solute elements remained in the matrix in all conditions. The matrix level in the 12YW alloy heat treated for 10 h at 1300 °C was similar to the other conditions indicating that the solute in the precipitates was not dissolved in the matrix. These high levels should produce

a significant amount of solid solution hardening. The composition was found to vary significantly between one region and another, as is indicated by the magnitude of the standard deviation of the measurements. This variation may be due to local inhomogeneities due to the mechanical processing, remnants of surface films, or remnants of solute segregation to dislocations and grain boundaries. The matrix composition did not change significantly with processing condition. In all cases, the Y and O levels in the ferrite matrix were significantly higher than the equilibrium levels even after annealing for 10 h at 1300 °C [14].

Table 5. The matrix composition of the as-processed, crept and heat treated materials. The balance of these analyses was iron.

Matrix		Cr	W	Y	Ti	O
12 YW	As-processed	12.5 ± 0.04	0.68 ± 0.01	0.03 ± 0.002	0.05 ± 0.003	0.19 ± 0.005
	10 h 1300°C	12.2 ± 0.07	0.89 ± 0.02	0.07 ± 0.006	0.10 ± 0.007	0.11 ± 0.007
12 YWT	As-processed	12.8 ± 0.11	0.79 ± 0.03	0.01 ± 0.004	0.08 ± 0.01	0.11 ± 0.01
	Crept 650°C	11.1 ± 0.31	0.28 ± 0.05	0.10 ± 0.03	0.13 ± 0.04	0.17 ± 0.04
	Crept 800°C	12.3 ± 0.08	0.65 ± 0.02	0.06 ± 0.01	0.11 ± 0.01	0.17 ± 0.01
	Crept 850°C MS	10.8 ± 0.02	0.90 ± 0.01	0.12 ± 0.003	0.14 ± 0.003	0.19 ± 0.003
	Crept 850°C	12.3 ± 0.07	0.59 ± 0.01	0.02 ± 0.003	0.09 ± 0.01	0.12 ± 0.01
	10 h 1300°C	12.7 ± 0.08	0.84 ± 0.02	0.10 ± 0.008	0.09 ± 0.01	0.10 ± 0.01

Many different types of molecular ions including TiO_2^+ , CrO_2^+ , WN_2^+ , WN_3^+ , WO_2^+ and WO_3^+ were observed in the atom probe analyses of both the particles and the matrix regions. These molecular ions indicate that the oxygen and solute elements were strongly associated in the alloy since they field evaporated together. However, their detection should not be taken as conclusive proof of a nearest neighbor arrangement as it is possible for surface diffusion to occur under the influence of the high electrical field prior to field evaporation. This observation confirms the expected strong affinity of the oxygen for the other solute atoms in the matrix. This affinity would have a significant influence on the diffusion of both the oxygen and other solute atoms because the oxygen and the solutes would either have to either break their mutual association or diffuse as a complex species. Both these processes would be energetically unfavorable and may effectively retard or inhibit solute diffusion. These oxygen-solute complexes would also have some influence on the mechanical properties due to their interaction with dislocations.

The measured oxygen level in the matrix was close to that of the alloy composition. As oxygen is also present in the particles, an additional source of oxygen must account for the higher measured total oxygen level. Since these materials were fabricated from fine powders, a thin oxide film or absorbed gases on the surface of the powder could introduce a significant amount of oxygen into the system. To investigate this possibility, a freshly electropolished needle of the 12YWT alloy was characterized in the atom probe after approximately 2 min. exposure to air. This characterization revealed a 2-nm-thick oxide film on the surface. The formation of such a surface film on the pre-alloyed powder may account for the increase oxygen content of the as-processed material relative to the nominal composition of the alloy.

Conclusions

The results of this and previous atom probe tomography characterizations have revealed at least four possible contributions to the mechanical properties of these MA/ODS materials. These contributions include: precipitate hardening from the high number density of ultra-fine 4-nm-diameter Ti-, Y- and O-enriched particles; dislocation pinning due to solute segregation of Cr, W, Ti, Y, O, C and B to the vicinity of dislocations and the presence of oxygen-solute atom complexes; and solid solution strengthening from the high concentration of alloying elements in the ferrite matrix. The ultra-fine particles were stable during long term creep experiments at high temperatures and annealing at temperatures of up to 1300 °C. The Y and O levels in the ferrite matrix were significantly higher than the equilibrium levels. These results may be related to the O-Ti, O-W, O-Y and O-Cr solute atom interactions influencing solute diffusion.

Acknowledgements

The authors would like to thank Prof. K. Miyahara of the Department of Molecular Design, Nagoya University, Nagoya, Japan and Dr. J. Okuda, Kobe Special Tube Co. Ltd, Japan for the provision of the MA/ODS alloys used in this study, Dr. I-S. Kim, formerly at Nagoya University, Nagoya, Japan for his assistance in the creep tests and Drs. P. J. Maziasz, L. Heatherly and R. L. Klueh of Oak Ridge National Laboratory for their assistance. Research at the Oak Ridge National Laboratory SHaRE Collaborative Research Center was sponsored by the Laboratory Directed Research and Development Program and the Division of Materials Sciences and Engineering, U.S. Department of Energy, under contract DE-AC05-00OR22725 with UT-Battelle, LLC.

References

1. G. D. Smith and J. J. deBarbadillo, in *Structural Applications of Mechanical Alloying*, J. J. deBarbadillo, et al., ASM-International, Materials Park, OH (1994), pp. 117-123.
2. S. Ukai, M. Harada, H. Okada, M. Inoue, S. Nomura, S. Shikakura, K. Asabe, T. Nishida and M. Fujiwara, *J. Nucl. Mater.*, **204** (1993) 65.
3. S. Ukai, M. Harada, H. Okada, M. Inoue, S. Nomura, S. Shikakura, T. Nishida and M. Fujiwara, *J. Nucl. Mater.*, **204** (1993) 74.
4. S. Ukai, T. Nishida, H. Okada, T. Okuda, M. Fujiwara and K. Asabe, *J. Nucl. Sci Tech*, **34** (1997) 256.
5. S. Ukai, T. Yoshitake, S. Mizuta, Y. Matsudaira, S. Hagi and T. Kobayashi, *J. Nucl. Sci Tech*, **36** (1999) 710.
6. I-S. Kim, T. Okuda, C-Y. Kang, J-H. Sung, P. J. Maziasz, R. L. Klueh and K. Miyahara, *Metals and Materials*, **6** (2000) 513.
7. D. J. Larson, P. J. Maziasz, I-S. Kim and K. Miyahara, *Scripta Mater.*, **44** (2001) 359-364.
8. I-S. Kim, J. D. Hunn, N. Hashimoto, D. J. Larson, P. J. Maziasz, K. Miyahara and E. H. Lee, *J. Nucl. Mater.*, **280** (2000) 264.
9. E. A. Kenik, D.T. Hoelzer, P.J. Maziasz and M. K. Miller, *Microscopy and Microanalysis*, **7** (2001), 550.
10. M.K. Miller, E.A. Kenik, K. F. Russell, L. Heatherly, D.T. Hoelzer and P.J. Maziasz, *Mater. Sci. Eng. A*, in press.
11. M.K. Miller, *Atom Probe Tomography: Analysis at the Atomic Level*, Kluwer Academic/Plenum, New York, 2000.
12. J.M. Hyde, D. Phil thesis, University of Oxford, Oxford, UK, 1993.

13. R.L. Klueh, P.J. Maziasz, D.J. Larson, N. Hashimoto, L. Heatherly, M.K. Miller, I-S. Kim, and K. Miyahara, Fusion Materials Semiannual Progress Report, DOE/ER-0313/28, (2000), 123-130.
14. J.H. Swisher and E.T. Turkdogan, Trans. Met. Soc. AIME, 239 (1967) 426-31.